Chemotactic predator-prey dynamics

Ankush Sengupta, Tobias Kruppa, and Hartmut Löwen
Institut für Theoretische Physik II: Weiche Materie, Heinrich-Heine-Universität, Universitätsstrasse 1, D-40225 Düsseldorf, Germany
(Received 10 November 2010; revised manuscript received 17 January 2011; published 23 March 2011)

A discrete chemotactic predator-prey model is proposed in which the prey secrets a diffusing chemical which is sensed by the predator and vice versa. Two dynamical states corresponding to catching and escaping are identified and it is shown that steady hunting is unstable. For the escape process, the predator-prey distance is diffusive for short times but exhibits a transient subdiffusive behavior which scales as a power law $t^{1/3}$ with time t and ultimately crosses over to diffusion again. This allows us to classify the motility and dynamics of various predatory microbes and phagocytes. In particular, there is a distinct region in the parameter space where they prove to be infallible predators.

DOI: 10.1103/PhysRevE.83.031914 PACS number(s): 87.17.Jj, 05.40.−a, 05.10.Gg

I. INTRODUCTION

Phagocytes or predatory microbes hunt their prey by chemotaxis [1,2], i.e., they sense the concentration of a chemical which is secreted by the prey and diffuses through the solution [3]. Typically, the predator moves along the steepest gradient of the chemical concentration to ultimately find its ejection source. Likewise the prey (another microbe) "smells" a secreted chemical from the advancing predator and tries to escape by moving along in the opposite direction of its maximal gradient. For biological systems of such chemotactically coupled microorganisms, questions on how the physical parameters that describe the predator-prey relationship affect hunting are relevant not only for studying taxis behavior but also for the survival of the prey and competition among predators, where individual attributes and advantages can greatly vary. A few common microbial predators and phagocytes include *Bdellovibrio* [4–6], *Pseudomonas aeruginosa* [7], *Dictyostelium discoideum* [8,9], lymphocytes [10], alveolar macrophages [11], and *Myxococcus xanthus* [12,13]. The eukaryotic cells, being larger in size, can chemotax by direct gradient sensing of their local chemical environment [14], and in the present article we are concerned only with the spatial gradient-sensing scenario. It is argued that prokaryotes, like bacteria, due to their small size, are unable to detect spatial chemical gradients across their length [15] and can sense by temporal comparison of chemical concentrations [16]. However, the size limit for effective spatial gradient sensing has been shown to be smaller than a typical bacterium size [17], and a contribution from direct gradient sensing toward bacterial chemotaxis can be present under appropriate situations (like slow speed, a roundish shape, and high chemical concentration with a steep gradient) [17,18].

Previous theoretical investigations have focused on spatiotemporal pattern formation in predator-prey colonies [19,20] which are typically described by nonlinear reaction-diffusion equations [21–23]. While the latter approaches involve coarse-grained continuum modeling, there are far fewer model studies on *individual* microorganisms. A discrete swarming model of individual self-propelled particles for bacterial colonies has been proposed by Czirók *et al.* [19] based on experimental observations. This was elaborated recently by Romanczuk *et al.* [24] based on a related individual model of Schweitzer and Schimansky-Geier [25]. Finally, individual autochemotactic models have been studied where the microbe follows its own diffusing secretion [26–29]. In all of these individual models there is no predator involved, apart from a recent study [30] which addressed a lattice model with no chemicals involved. A recent experiment on eukaryotic chemical gradient sensing showed that cells can vary greatly in their response behavior even within a genetically identical population [31]. While the behavior of a single cell remained highly reproducible in repeated exposures to chemical pulses, the response magnitude was shown to vary from cell to cell for the same pulse, pointing out the importance of cell individuality in the context of chemotactic response.

Here we propose a discrete model which describes both the predator and the prey individually and contains explicitly the diffusion of the two chemicals secreted by the predator and the prey together with the Brownian motion of the latter. The deterministic (fluctuation-free) model is analyzed analytically and by numerical solution which is supplemented by Brownian dynamics computer simulations at finite temperature. Depending on the physical parameters describing the model and the initial distance between predator and prey, two different dynamical processes are identified which correspond to *catching* and *escaping* and an unstable *steady hunting*. Within the trapped phase, it is shown that there is a distinct regime of *no escape* where the prey's advantage in terms of its initial separation from the predator alone cannot decide the outcome. By analytical treatment, various scaling laws are extracted characterizing and delineating the different regimes. In the absence of noise, the mean-square distance between predator and prey scales with different exponents α as a function of time with a subdiffusive anomalous exponent $\alpha = 2/3$ for escaping [32] and a ballistic behavior $\alpha = 0$ for steady hunting. Brownian motion leads to ultimate diffusion ($\alpha = 1$) such that these exponents are transient. Catching is accompanied by a scaling form of $|t - t_{\rm cap}|^{\alpha}$, with $\alpha = 2/3$, and $t_{\rm cap}$ being the time taken by the predator to capture the prey. In principle, our results allow to map and classify different biological systems into the different regimes.

Our article is organized as follows: In Sec. II we describe the model, pointing out typical experimental situations to compare the estimates of the physical parameters used in our model. The results of our analysis, both from theory and simulations,

are presented in Sec. III, explaining the dynamical phase diagram and the different power laws for escaped and trapped situations. Finally, in Sec. IV, we discuss these results and point out situations where our findings can be important and counting.

II. MODEL

In our discrete predator-prey model, the predator is at position $\mathbf{r}_1(t)$ at time t, hunting the prey which is at position $\mathbf{r}_2(t)$ and trying to escape. The concentration field of the chemical secreted by the predator (prey) at a constant ejection rate $\lambda_{1(2)}$ is denoted by $c_{1(2)}(\mathbf{r},t)$. Assuming a gradient-sensing scenario for each microbe in response to the chemical secreted by the other, and taking into account effective stochastic fluctuations that are associated with the nonequilibrium self-propulsion mechanism of each, the overdamped equations of motion for the predator and the prey, respectively, read

$$\gamma_1 \dot{\mathbf{r}}_1 = +\kappa_1 \nabla c_2(\mathbf{r}_1,t) + \boldsymbol{\eta}_1(t) \quad (1)$$

$$\gamma_2 \dot{\mathbf{r}}_2 = -\kappa_2 \nabla c_1(\mathbf{r}_2,t) + \boldsymbol{\eta}_2(t). \quad (2)$$

Here, $\gamma_{1(2)}$, $\kappa_{1(2)}$, and $\eta_{1(2)}(t)$ are the damping constant in the medium, the chemical coupling constant (a measure of the gradient-sensing strength), and the effective noise vector associated with stochastic self-propulsion of the predator (prey), respectively. The first term on the right, in both equations, models the systematic contribution of chemotactic response through simple gradient sensing. We take both $\kappa_{1,2} > 0$ so c_2 acts as a chemoattractant for the predator, while c_1 is a chemorepellant for the prey. We model $\eta_i(t)$ as a Gaussian white noise: $\langle \eta_i(t) \rangle = \mathbf{0}$, $\langle \eta_{i\mu}(t)\eta_{j\nu}(t') \rangle = 2\gamma_i \beta^{-1} \delta_{ij}\delta_{\mu\nu}\delta(t - t')$. The Greek indices refer to spatial components, while the Roman indices are reserved for the microbe's attributes ($i = 1$ denotes predator, whereas 2 denotes prey). Here, β corresponds to an inverse effective temperature associated with the stochastic fluctuations, such that $D_i = 1/(\gamma_i \beta)$ is the nonchemotactic diffusion constant of the microbe concerned. Hydrodynamic interaction between the microbes is neglected.

The diffusion equation of each of the chemicals reads

$$\frac{\partial c_i(\mathbf{r},t)}{\partial t} + \mathbf{u}_i(\mathbf{r},t) \cdot \nabla c_i(\mathbf{r},t) = D_{\rm ci} \nabla^2 c_i(\mathbf{r},t) + \lambda_i \delta[\mathbf{r} - \mathbf{r}_i(t)], \quad (3)$$

where $D_{\rm ci}$ is the diffusivity of the corresponding chemical, and we have assumed each microbe as a point-source emitter. $\mathbf{u}_i(\mathbf{r},t)$ is the advective flow-field set in the medium due to the motion of the microbe. Spatial gradient-sensing microbes are known to move slowly with velocity on the order $v \sim 10^{-2}$–10^{-1} μm/s and are typically of size $a \sim 1$–10 μm. Chemicals are secreted typically at $\lambda_i \sim 10^3$ molecules/s and diffuse at $D_{\rm ci} \sim 10^2$–10^3 μm^2/s. Under such practical situations, noting that the magnitude of the flow-field $|\mathbf{u}_i|$ can be at most on the order of v, the Péclet number for the problem is $av/D_{\rm ci} \sim 10^{-5}$–$10^{-2}$. This makes the advective term negligible, and the chemical diffusion equation reduces to

$$\frac{\partial c_i(\mathbf{r},t)}{\partial t} - D_{\rm ci} \nabla^2 c_i(\mathbf{r},t) = \lambda_i \delta[\mathbf{r} - \mathbf{r}_i(t)]. \quad (4)$$

Fast-moving microorganisms with $v \sim 10$–10^2 μm/s (capable of producing appreciable advection in the medium) are known to chemotax by "temporal sensing" mechanism of the chemical concentration [16] which we do not address here.

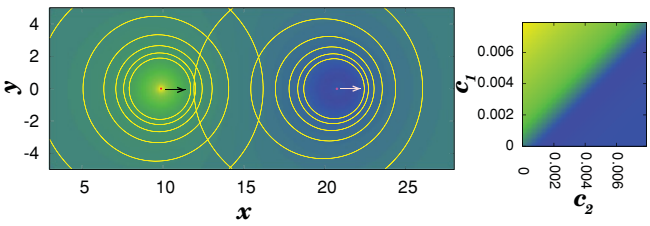

FIG. 1. (Color online) (Left) Chemotactic chase: A predator (red dot on left) chases a prey (red dot on right), while the latter tries to escape through chemotactic gradient sensing of the diffusing chemicals. The arrows indicate their respective direction of motion in the absence of fluctuations. The contours around each microbe represent the equiconcentration lines of the secreted chemicals in a two-dimensional projected plane in this case, indicating the asymmetry of the distribution. The color code used here for the spatial distribution of the secreted chemorepellant (c_1) and the chemoattractant (c_2), as they mingle in space, is shown in the right panel.

For an unconfined space in three dimensions, the Green's function solution to Eq. (4) yields

$$c_i(\mathbf{r},t) = \lambda_i \int_0^t dt' \frac{1}{(4\pi D_{\rm ci}|t - t'|)^{\frac{3}{2}}} \exp\left\{ \frac{-[\mathbf{r} - \mathbf{r}_i(t')]^2}{4D_{\rm ci}|t - t'|} \right\}. \quad (5)$$

Brownian dynamics of the predator-prey system is implemented to simulate the chemotactic motion [Eqs. (1) and (2)] and we used Eq. (5) to calculate the spatial gradient of the chemical concentration. We measured time in units of λ_2^{-1}, lengths in units of $l_0 = 0.1\sqrt{D_{c2}/\lambda_2}$, and energy in units of $\epsilon_0 = \gamma_2 D_{c2}$. Real estimate yields $\kappa_i \sim 10^3 \epsilon_0 l_0^3$ for *Dictyostelium* [9] moving at 0.2 μm/s up the cAMP gradient of 0.01 nM/μm, secreted at 10^3 molecules/s with diffusivity 300 μm^2/s. Microglial cells [33] moving at 2 μm/min in response to an interleukin gradient of 0.003 nM/μm secreted at 200 molecules/min and diffusing at 900 μm^2/min has $\kappa_i \sim 10\epsilon_0 l_0^3$.

III. RESULTS AND ANALYSIS

A first look at the problem suggests that in addition to the chemical diffusivities, the attributes of the individual microbes, viz., their mobility, chemical ejection rates, and gradient-sensing strengths, as well as the predator's advantage in terms of its initial distance from the prey, $r_0 = r_{12}(t = 0) \equiv |\mathbf{r}_2(0) - \mathbf{r}_1(0)|$, combined, will be deciding factors. Thus, the fate of the prey, i.e., whether it will be captured, can escape, or will be steadily hunted for ever, depends on a multitude of parameters. Having set the model, it is therefore instructive to examine the zero-noise [$\boldsymbol{\eta}_i(t) = \mathbf{0}$] deterministic case first, in order to understand the combination of variables relevant in predicting the outcome. Figure 1 shows a simulation snapshot of the chemotactic chase process in the absence of fluctuations. Assuming a steady-state velocity v_i for microbe i, moving

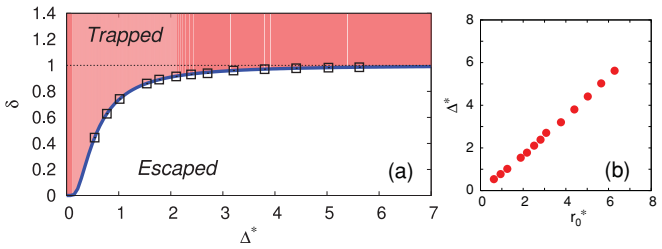

FIG. 2. (Color online) (a) Dynamical phase diagram of the chemotactic predator-prey system, constructed in the Δ^*-δ parameter space, showing the trapped (shaded) and escaped phases. The phase boundary (thick solid line) is obtained analytically and matches the simulation data (boxes). The horizontal thin dotted line ($\delta = 1$) represents the upper bound for the trapped-to-escaped dynamical phase transition (see text). (b) The dependence of the catching range (Δ^*) on the initial separation ($r_0{}^*$), as obtained from simulations.

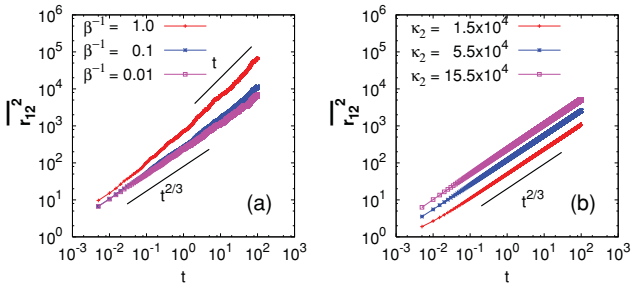

FIG. 3. (Color online) Mean-squared displacement of the prey with respect to the predator as a function of time, with $\lambda_1 = 1$, $\gamma_1 = 10$, $\gamma_2 = 0.01$, $D_{c1} = 10^3$, $D_{c2} = 10^2$, $\kappa_1 = 10^4$ for (a) $\beta^{-1} = 1.0, 0.1, 0.01$ (top to bottom) and $\kappa_2 = 15.5 \times 10^4$; (b) the zero noise case ($\beta^{-1} = 0$) and $\kappa_2 = 1.5 \times 10^4$, 5.5×10^4, 15.5×10^4 (bottom to top). The power-law behaviors $t^{2/3}$ and t are illustrated by the corresponding reference lines.

along the x axis, the concentration profile for the chemical secreted by it simplifies to

$$c_i(\mathbf{r}, t = 0) = (\lambda_i / 2\pi D_{\rm ci} r) \exp[(-v_i(x + r)/2D_{\rm ci}]. \quad (6)$$

In the presence of chemotactic coupling, one then expects $\gamma_i v_i = (1 - \delta_{ij})\kappa_i [\partial c_j(\mathbf{r})/\partial x]_{\mathbf{r}=\mathbf{r}_{ij}}$ for each of them. In addition, demanding a condition for steady hunting, whence $v_i = v_j$, maintaining a constant separation $r_{12} = \Delta$, leads to

$$\delta(\Delta^*) = (1 + \Delta^{*-1}) \exp(-\Delta^{*-1}). \quad (7)$$

Here, $\Delta^* = \Delta/\Delta_0$, $\Delta_0 = \kappa_1\lambda_2/(4\pi D_{c1} D_{c2}\gamma_1)$, being a length scale, and $\delta = (\kappa_1\gamma_2\lambda_2 D_{c1})/(\kappa_2\gamma_1\lambda_1 D_{c2})$ will be termed a *sensibility ratio* in the predator-prey relationship. Figure 2(a) shows the resulting phase diagram. For a given Δ^*, if the sensibility ratio is increased, there is a transition from the escaped (free) to the trapped (capture) phase. To understand this we note that an increase in the chemoattractant coupling or its emission or a decrease of the prey's mobility would prove advantageous to the predator in sensing the prey at a given distance. Also, a decrease in the chemoattractant diffusivity will enable the predator to easily track its prey and ultimately trap it. Similarly, for a given δ, increase in the separation distance will be advantageous to the prey in escaping. Further, since $\Delta > 0$ (predator follows prey), the validity of Eq. (7) requires $\delta < 1$. This implies that the phase boundary between the trapped and escaped state lies below the $\delta(\Delta^*) = 1$ line in the parameter space. For $\delta \geqslant 1$, there is *no escape*; whatever the separation between the microbes, the predator will ultimately capture the prey in this case.

In our simulations, the control parameter is the initial distance, r_0, between predator and prey. By tuning δ for a given r_0, we actually found the point of transition from trapped to escaped state. The borderline case of steady hunting was found to be unstable. Close to the borderline situation, the predator-prey distance r_{12} remains constant for a long time before fluctuations throw them into either the trapped or the escaped state. This constant distance, if identified with Δ, matches the phase boundary [Eq. (7)] perfectly, and Δ^* depends on $r_0^*(= r_0/\Delta_0)$ in a roughly linear fashion [Fig. 2(b)].

What are the dynamical features of the escaped and the trapped phases? Our simulations show that for escape [Fig. 3(a)], the mean-squared displacement of the prey with respect to the predator gradually deviates from the initial value, r_0, and grows subdiffusively with time as $\overline{\mathbf{r}_{12}{}^2} \sim t^\alpha$, with an exponent $\alpha = 2/3$, where the bar denotes an averaging over noise for a given r_0. This behavior finally crosses over to diffusion, $\overline{\mathbf{r}_{12}{}^2} \sim t$, for long times. The crossover time $t_{\rm co}$ decreases with increasing fluctuation strength β^{-1}. Zero-noise simulations show the subdiffusive motion as the final long-time behavior, with the same exponent α [Fig. 3(b)]. This implies that within this phase, the hunting process continues with a subdiffusive dynamics of the prey in the comoving frame of the predator; but, due to the effects of fluctuation, the prey finally diffuses away freely. It is therefore appropriate to look for a theoretical estimate of α within the noiseless ideal case. We note from Eq. (6) that at the advancing predator position, the chemoattractant profile behind the prey is of the form $c_2(|x|) = \lambda_2/(4\pi D_{c2}|x|)$ in the steady-state condition, since $x < 0$. Solving the resulting equation of motion in steady state, $\gamma_1 \dot{x} = \kappa_1 |\nabla c_2(x)|$, gives $x^2 \sim t^{2/3}$, explaining the subdiffusive exponent. When the fluctuations ultimately overcome the chemotactic coupling, crossover to final diffusion results, requiring $\beta^{-1} = \kappa_1 c_2(|x|) = \kappa_1\lambda_2/(4\pi D_{c2}|x|)$. At the crossover point from subdiffusive to the diffusive regime, $x(t = t_{\rm co}) \sim {t_{\rm co}}^{1/3}$; implying that the crossover time scales with the inverse effective temperature as $t_{\rm co} \sim \beta^3$.

At the front of each microbe, on the other hand, the respective chemical profile decays much faster $\sim \frac{1}{x} \exp(-v_i x/D_{\rm ci})$. The predator is thus always at an advantage of sensing the prey from much longer distances. Therefore, for very low δ, a small increase in δ greatly increases the catching range for the predator. This accounts for the almost vanishing slope of the phase boundary for low δ in the dynamical phase diagram [Fig. 2(a)]. In this part of the phase diagram, for two predators with a close sensibility ratio, the one with the slightly larger δ will successfully trap prey which were initially much further away. For intermediate values of δ, the catching range Δ^* increases at a slower rate with increase in δ. This is because the initial separation is large enough that small changes in Δ^* do not appreciably increase the chemoattractant gradient

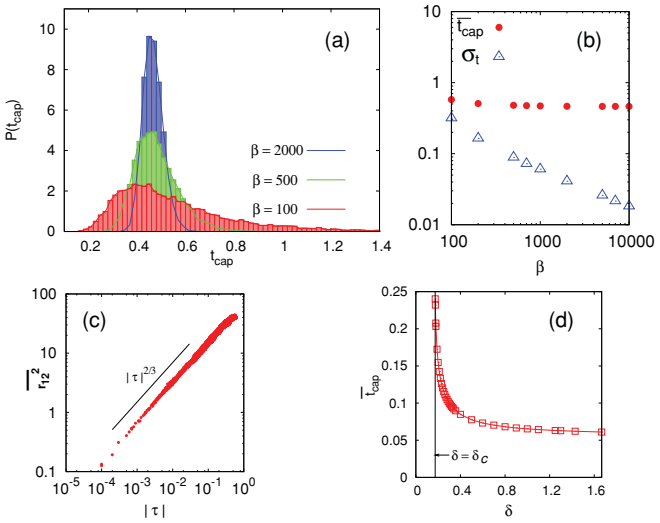

FIG. 4. (Color online) (a) Probability distribution of the capture time for the typical values of δ and Δ^* inside the trapped phase, for $\beta = 100, 500, 2000$, with $\lambda_1 = 1, \gamma_1 = 10, \gamma_2 = 10, D_{c1} = 10, D_{c2} = 10, \kappa_1 = 10^4, \kappa_2 = 500, r_0{}^* = 1.59155$. (b) Mean capture time ($\bar{t}_{\rm cap}$) and variance (σ_t) of the capture time, as a function of β. (c) Mean-squared predator-prey separation ($\overline{\mathbf{r}_{12}{}^2}$), close to trapping situations, as a function of the time interval $|\tau| = |t - t_{\rm cap}|$. The thick reference line indicates $\tau^{2/3}$ power-law behavior. (d) Divergence of the capture time with decrease in δ, for a fixed catching range (Δ^*), as the trapped-to-escape transition ($\delta = \delta_c$, shown by the vertical line) is approached. The parameters used are $\lambda_1 = 1, \gamma_1 = 10, \gamma_2 = 10, D_{c1} = 5, D_{c2} = 5, \kappa_1 = 10^4, r_0{}^* = 0.31416$, and $\delta_c = 0.17342$.

($\sim 1/x^2$) for the predator. One then needs to considerably alter the sensibility ratio for obtaining a significant change in the chemotactic coupling. As δ is further increased, Δ^* increases to diverge at $\delta = 1$.

For the trapping situation we find a broad skewed distribution [$P(t_{\rm cap})$] of capture time, $t_{\rm cap}$, for a fixed β, r_0, and δ [Fig. 4(a)]. The mean capture time $\bar{t}_{\rm cap}$ is, however, independent of the effective fluctuation strength, while the variance $\sigma_t = [\overline{(t_{\rm cap} - \bar{t}_{\rm cap})^2}]^{1/2}$ decreases with increasing β [Fig. 4(b)] on keeping the other parameters unchanged. The trapping dynamics also show nontrivial power-law behavior, very close to capture: $\overline{\mathbf{r}_{12}{}^2}(\tau \to 0-) \sim |\tau|^{2/3}$, where $\tau = t - t_{\rm cap}$ [Fig. 4(c)]. We note that initially, close to $t = 0$, when the predator-prey distance is $\sim r_0$, fluctuations dominantly control the individual microbe's motion until a steady chemical concentration profile sets up in the process to favor a systematic dynamics. This time scale depends on the individual diffusivities of the chemical. When the chemical diffusivities are higher compared to those of the nonchemotactic diffusivities of the microbes, the faster the predator-prey systematics will set in. For trapping dynamics that are very close to capture, therefore, the predator is already responding to the steady chemoattractant gradient, $\gamma_1 \dot{x} = \kappa_1 |\nabla c_2(r)|_{r=x} \sim 1/x^2$. Thus, integrating the equation of motion up to final capture, we obtain the scaling form $x^2 \sim (t_{\rm cap} - t)^{2/3}$, with $t < t_{\rm cap}$. For fixed initial separation, $\bar{t}_{\rm cap}$ diverges on approaching the corresponding critical value of the sensibility ratio (δ_c) for escape from above [Fig. 4(d)].

IV. DISCUSSIONS

In this article, we studied the dynamics of gradient-sensing chemotactic microorganisms in a predator-prey relationship. Although prokaryotes like most bacteria chemotax chiefly through a temporal comparison of chemical concentrations, the direct spatial sensing of a local chemical gradient studied here is prevalent among eukaryotes like amoeba, yeast cells, neutrophils, lymphocytes, and glial cells. Finding distinct dynamical signatures in chemotactic hunting and criteria for determining the trap and escape situations in these systems are important questions that can help understand, for example, survival of a prey [30,34], nutrient uptake, dynamics of macrophages [11] in antimicrobial defense, and perhaps the selection strategies for predator(s) when several signaling sources are present (e.g., prey colony [13] or chemical targets [35]). Our studies have shown when and when not the initial predator-prey separation counts in concluding the hunt, in combination with the many parameters involved, even at the level of a single predator and a prey. These basic features at the discrete individual level should, therefore, also be playing a part when collective motion in microbial colonies is involved and complex emergent phenomena are expected [11,13,31]. Rippling behavior in a cell population of *M. xanthus* predataxing through an *Escherichia coli* colony, for instance, has been explained by the predators' effort to maintain close contact with each other to achieve maximum glide velocity, counterbalanced by the tendency of each individual to achieve maximum feeding potential by directed movement to enhance contact with prey cells [13]. Thus, it remains to be seen whether an interplay between the distinct subdiffusive and diffusive time scales observed in the escape regime in our model can give rise to complex patterns in a chemotactic gradient-sensing predator-prey colony with varying predator-prey distances and, perhaps, with a variation in individual attributes.

The search time of an individual predator for its prey [36] is limited by its life span (e.g., a sperm cell in search for the egg cell within its lifetime); a hunt for an indefinite period is impractical. How the target capture time and its statistics depend on the amount of fluctuation in the system and the sensibility ratio, which we considered here, is thus of practical interest. Recently, a lattice model for group chase and escape in two dimensions has been formulated [37]. The model considers simple predation and evasion rules for the individuals and shows complex behaviors like the existence of an optimal number of predators, for a given number of prey, to maximize success of the catch, as well as the self-organized spatial structures that emerge. Though no explicit chemical sensing was involved in the model, the lifetime statistics of all targets (prey), taken together, shows a broad skewed distribution with a peak at the mean typical survival time, as also seen in our chemotactic system, and a sharp peak at unit time. The additional sharp peak was a result of targets positioned just next to some of the predators in the initial condition and caught in the next step. This also indicates that the initial predator-prey separation is, indeed, an important factor to consider. Understanding the dependence of capture time on cell motility is significant, for example, in estimating cell-target encounter rates in the immune response dynamics of neutrophils and macrophages. A mathematical

model for the cell-target encounter time was proposed in Refs. [38] and [39] to investigate phagocytosis of alveolar macrophages over pathogens on lung surface and for system of neutrophils inside three-dimensional tissues. This was based on different probability considerations for forward, backward, and transverse moves of the cell in its chemotactically biased motion. The resulting average encounter time was shown to rapidly decrease with an increase in the the probability of the forward move and with the chemotactic index defined as the ratio of the net displacement of the cell toward the target to the actual total distance traveled. This is qualitatively similar to the sharp decrease in the mean capture time with the increase in sensibility ratio in our model. In Ref. [38] it was further noted that although a modest degree of chemotactic bias reduced the mean encounter time by orders of magnitude, there was very little additional benefit for nearly perfect bias. This is also similar to our finding that the mean capture time is not affected by fluctuations in the system for a given sensibility ratio and a fixed initial distance, clearly identifying the parameters on which the capture time will depend when chemotaxis and random motility are both involved. The only benefit from a more perfect bias (less fluctuations), we observed, is in making the capture time more well defined and sharper by reducing the distribution width. While the cell-target encounter rate models were examined for fixed target positions or, at best, for randomly moving targets when averaging over all possible cell-target distances were considered, our model also explores the condition of finite sensibility ratio when the prey can as well be chemosensitive to the advancing predator and when escape might be possible. Given that it is by now possible to detect the individual and collective motion of cells simultaneously [11], we believe that our predictions should be experimentally verifiable in various biological systems. Chemically driven "microbots" [40], phoretic "chuckers" [41], and chemotactic nonbiological rods [42] are recently being studied through experiments and simulations for their convincing similarities with dynamics in the biological microworld. These elements self-propel in direct response to concentration gradients and should be ideal candidates for realizing our model outside the biological domain.

We have been able to delineate power-law behaviors in the chasing process, both from theory and numerical simulations, and crossover time scaling with fluctuation strength. A dynamical phase diagram has been obtained to identify conditions for escape and catching, with a borderline unstable steady-hunting situation ("win-win situation"). A broad class of phagocytic cells and microorganisms varying widely with respect to their mobility, secretion rates, and diffusivities of ejected chemicals and strength of spatial gradient sensing of chemicals, can be located on the phase diagram. Interestingly, a sensibility ratio resulting from our model calculation allows a criterion to predict the outcome of such hunting processes: a trapped or an escaped situation depending on the initial predator-prey separation and a no escape situation independent of their initial separation.

ACKNOWLEDGMENTS

We thank S. van Teeffelen, P. Romanczuk, M. S. Roy, P. S. Hammond, and R. Winkler for helpful discussions. This work was supported by DFG within SFB TR6 (project D3).

[1] M. Kollmann, L. Lovdok, K. Bartholome, J. Timmer, and V. Sourjik, Nature **438**, 504 (2005).
[2] U. B. Kaupp, N. D. Kashikar, and I. Weyand, Annu. Rev. Physiol. **70**, 93 (2008).
[3] W. C. K. Poon, in *Soft Matter: From Synthetic to Biological Materials*, Lecture Notes of the 39th IFF Spring School (Forschungszentrum Julich GmbH, Germany, 2008), Vol. D11, pp. 1–15.
[4] M. E. Nunez, M. O. Martin, P. H. Chan, and E. M. Spain, Colloids Surf. B **42**, 263 (2005).
[5] E. Strauch, D. Schwudke, and M. Linscheid, Future Microbiol. **2**, 63 (2007).
[6] M. Dori-Bachash, B. Dassa, S. Pietrokovski, and E. Jurkevitch, Appl. Environ. Microbiol. **74**, 7152 (2008).
[7] J. Kato, H. E. Kim, N. Takiguchi, A. Kuroda, and H. Ohtake, J. Biosci. Bioeng. **106**, 1 (2008).
[8] M. Clarke and L. Maddera, Eur. J. Cell Biol. **85**, 1001 (2006).
[9] R. G. Endres and N. S. Wingreen, Proc. Natl. Acad. Sci. USA **105**, 15749 (2008).
[10] S. H. Zigmond, J. Cell Biol. **75**, 606 (1977).
[11] B. E. Farrell, R. P. Daniele, and D. A. Lauffenburger, Cell Motil. Cytoskel. **16**, 279 (1990).
[12] D. P. Astling, J. Y. Lee, and D. R. Zusman, Mol. Microbiol. **59**, 45 (2006).
[13] J. E. Berleman, J. Scott, T. Chumley, and J. R. Kirby, Proc. Natl. Acad. Sci. USA **105**, 17127 (2008).
[14] H. C. Berg and E. M. Prucell, Biophys. J. **20**, 193 (1977).
[15] R. M. Macnab and J. D. E. Koshland, Proc. Natl. Acad. Sci. USA **69**, 2509 (1972).
[16] J. E. Segall, S. M. Block, and H. C. Berg, Proc. Natl. Acad. Sci. USA **83**, 8987 (1986).
[17] D. B. Dusenbery, Biophys. J. **74**, 2272 (1998).
[18] R. Thar and M. Kühl, Proc. Natl. Acad. Sci. USA **100**, 5748 (2003).
[19] A. Czirók, E. Ben-Jacob, I. Cohen, and T. Vicsek, Phys. Rev. E **54**, 1791 (1996).
[20] M. E. Boraas, D. B. Seale, and J. E. Boxhorn, Evol. Ecol. **12**, 153 (1998).
[21] E. F. Keller and L. A. Segel, J. Theor. Biol. **30**, 225 (1971).
[22] M. A. Tsyganov, J. Brindley, A. V. Holden, and V. N. Biktashev, Phys. Rev. Lett. **91**, 218102 (2003).
[23] P. Y. H. Pang and M. X. Wang, J. Diff. Equ. **200**, 245 (2004).
[24] P. Romanczuk, U. Erdmann, H. Engel, and L. Schimansky-Geier, Eur. Phys. J. Special Topics **157**, 61 (2008).
[25] F. Schweitzer and L. Schimansky-Geier, Physica A **206**, 359 (1994).
[26] Y. Tsori and P.-G. de Gennes, Europhys. Lett. **66**, 599 (2004).
[27] R. Grima, Phys. Rev. Lett. **95**, 128103 (2005).

[28] R. Grima, Phys. Rev. E **74**, 011125 (2006).
[29] A. Sengupta, S. van Teeffelen, and H. Löwen, Phys. Rev. E **80**, 031122 (2009).
[30] G. Oshanin, O. Vasilyev, P. L. Kraapivsky, and J. Klafter, Proc. Natl. Acad. Sci. USA **106**, 13696 (2009).
[31] A. Samadani, J. Mettetal, and A. van Oudenaarden, Proc. Natl. Acad. Sci. USA **103**, 11549 (2006).
[32] For anomalous diffusion in active particles, see, e.g., R. Golestanian, Phys. Rev. Lett. **102**, 188305 (2009).
[33] M. Luca, A. Chavez-Ross, L. Edelstein-Keshet, and A. Mogilner, Bull. Math. Biol. **65**, 693 (2003).
[34] S. Yair, D. Yaacov, K. Susan, and E. Jurkevitch, Agronomie **23**, 433 (2003).
[35] S. A. Nowak, B. Chakrabarti, T. Chou, and A. Gopinathan, Phys. Biol. **7**, 026003 (2010).
[36] B. M. Friedrich, Phys. Biol. **5**, 026007 (2008).
[37] A. Kamimura and T. Ohira, New J. Phys. **12**, 053013 (2010).
[38] E. S. Fisher and D. A. Lauffenburger, Biophys J. **51**, 705 (1987).
[39] S. B. Charnick and D. A. Lauffenburger, Biophys. J. **57**, 1009 (1990).
[40] A. Sen, M. Ibele, Y. Hong, and D. Velegol, Farady Discuss. **143**, 15 (2009).
[41] C. Valeriani, R. J. Allen, and D. Marenduzzo, J. Chem. Phys. **132**, 204904 (2010).
[42] Y. Hong, N. M. K. Blackman, N. D. Kopp, A. Sen, and D. Velegol, Phys. Rev. Lett. **99**, 178103 (2007).